Journal of Medicinal Chemistry

ARTICLE

pubs.acs.org/jmc

Structure−Activity Relationship and Multidrug Resistance Study of New *S*-trityl-L-Cysteine Derivatives As Inhibitors of Eg5†

Hung Yi Kristal Kaan,[‡] Johanna Weiss,[§] Dominik Menger,[§] Venkatasubramanian Ulaganathan,[‡] Katarzyna Tkocz,[‡] Christian Laggner,[⊥] Florence Popowycz,[∥] Benoît Joseph,[∥] and Frank Kozielski*[,‡]

[‡]The Beatson Institute for Cancer Research, Switchback Road, Bearsden, Glasgow G61 1BD, Scotland, U.K.

[§]University Hospital Heidelberg, Department of Clinical Pharmacology and Pharmacoepidemiology, Im Neuenheimer Feld 410, D-69120 Heidelberg, Germany

[∥]Institut de Chimie et Biochimie Moléculaires et Supramoléculaires, UMR-CNRS 5246, Université de Lyon, Université Claude Bernard−Lyon 1, Bâtiment Curien, 43, Boulevard du 11 Novembre 1918, F-69622 Villeurbanne, France

[⊥]Institute of Pharmacy, Department of Pharmaceutical Chemistry and Center for Molecular Biosciences Innsbruck (CMBI), University of Innsbruck, Innrain 52c, 6020 Innsbruck, Austria

Supporting Information

ABSTRACT: The mitotic spindle is a validated target for cancer chemotherapy. Drugs such as taxanes and vinca alkaloids specifically target microtubules and cause the mitotic spindle to collapse. However, toxicity and resistance are problems associated with these drugs. Thus, alternative approaches to inhibiting the mitotic spindle are being pursued. These include targeting Eg5, a human kinesin involved in the formation of the bipolar spindle. We previously identified *S*-trityl-L-cysteine (STLC) as a potent allosteric inhibitor of Eg5. Here, we report the synthesis of a new series of STLC-like compounds with in vitro inhibition in the low nanomolar range. We also performed a multidrug resistance study in cell lines overexpressing P-glycoprotein and showed that some of these inhibitors may have the potential to overcome susceptibility to this efflux pump. Finally, we performed molecular docking of the compounds and determined the structures of two Eg5−inhibitor complexes to explain the structure−activity relationship of these compounds.

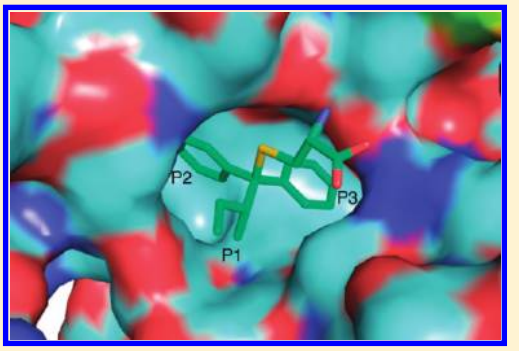

INTRODUCTION

Mitosis is a highly regulated process whereby duplicated chromatids are equally distributed to daughter cells. While regulated cell proliferation is essential for the maintenance of life, uncontrolled cell proliferation, a characteristic of cancer cells, gives rise to tumors. Drugs like taxanes and vinca alkaloids belong to a group of successful anticancer drugs that possess antitumor properties by impeding mitosis and cell proliferation. These drugs specifically target tubulin, the building block of microtubules, thus interfering with microtubule dynamics and resulting in the collapse of the mitotic spindle.

However, some tumors/tumor cell lines may develop drug resistance, de novo or acquired, against tubulin targeting drugs through a variety of putative mechanisms, including the expression of point mutations in tubulins, overexpression of certain tubulin isoforms that are able to evade drug treatment, or multidrug resistance (MDR).[1−3] The best-known and probably the most important transporter for MDR is P-glycoprotein (Pgp, encoded by *ABCB1*), an efflux pump present in many tissues and tumors that has a very broad substrate specificity and is capable of eliminating xenobiotics such as taxanes and vinca alkaloids from the cell.[4] To fight these liabilities associated with current treatments, efforts are underway to develop improved tubulin targeting drugs with reduced susceptibility to MDR. A second important strategy currently pursued is the validation of other essential mitotic spindle proteins as potential new targets for cancer chemotherapy.[5,6] These potential new targets belong to two major protein families, namely mitotic kinases such as PLK1 and the auroras[7,8] and certain members of the kinesin superfamily such as Eg5 (Kif11, a member of the kinesin-5 family) and CENP-E (Kif10, a member of the kinesin-7 family).[9]

Eg5 is an essential mitotic kinesin involved in the establishment of the bipolar spindle.[10] A variety of Eg5 inhibitors are currently investigated in view of their potential as antimitotic agents with antitumor activity.[6] Because of the restricted function of mitotic kinesins, Eg5 inhibitors do not induce neurotoxicity, a liability observed with many tubulin targeting drugs.[11] Because they operate by a different mechanism of action compared to tubulin inhibitors, these inhibitors can also overcome resistance that are caused by mutations in tubulin or overexpression of different tubulin isoforms. On the other hand, MDR due to the

Received: August 2, 2010
Published: February 23, 2011

Scheme 1[a]

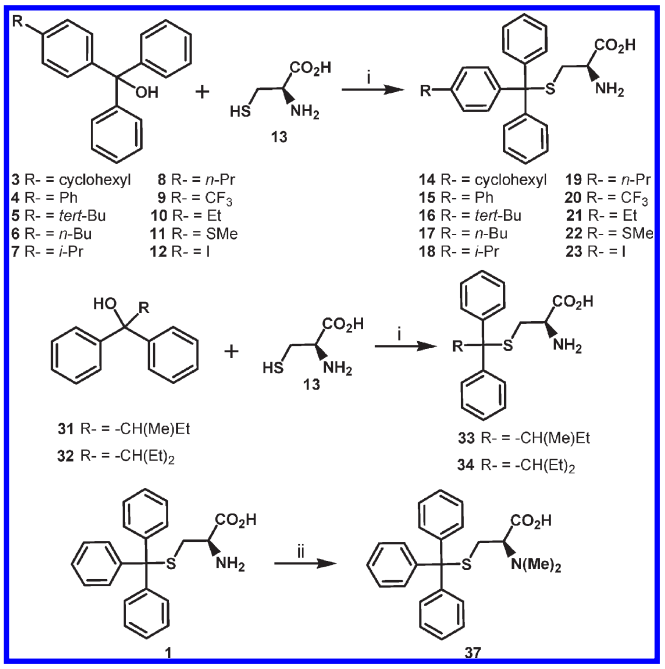

[a] Reagents and conditions: (i) $BF_3 \cdot Et_2O$, AcOH, rt, 2 h, **14** = 36%, **15** = 21%, **16** = 30%, **17** = 35%, **18** = 31%, **19** = 40%, **20** = 29%, **21** = 25%, **22** = 33%, **23** = 20%, **33** = 35%, **34** = 37%; (ii) HCHO 37% in water, $NaBH(OAc)_3$, MeOH, 0 °C to rt, 24 h, **37** = 19%.

overexpression of Pgp is independent of the mode of action of a drug and thus can be a liability for Eg5 targeting drugs. Therefore, potential Eg5 inhibitors should be tested for their susceptibility to the Pgp efflux pump and investigated for their effectiveness in MDR (Pgp overexpressing) cells.

Our group had previously identified a triphenylmethyl compound, *S*-trityl-L-cysteine (**1**) (STLC), as a potent inhibitor of human mitotic Eg5.[12] Using an in vitro screening procedure based on the inhibition of the ATPase activity of Eg5,[13] we showed that STLC is a tight-binding inhibitor which inhibits the ATPase activity of Eg5 in the low nanomolar range, with an estimated K_i^{app} of 25−100 nM, and induces mitotic arrest with an MI_{50} of about 700 nM in HeLa cells.[14] STLC works by slowing ADP release from the catalytic site of Eg5. In HeLa cells, STLC induces a prolonged mitotic arrest, which eventually leads to cell death by the intrinsic apoptotic pathway.[15] Two structure−activity relationship (SAR) studies have been performed, leading to the identification of the STLC pharmacophore and the synthesis of more active compounds with MI_{50} values in the range of 150 to 200 nM in cell-based assay. The best compounds carry an additional functional group in the *para*-position of one or two of the phenyl rings.[16,17]

To expand our knowledge of the drug-like properties and efficacy of STLC-like compounds, we synthesized and investigated a novel set of *para*-substituted analogues by measuring the inhibition of the basal and MT-stimulated Eg5 ATPase activities. We then selected a set of representative *para*-substituted analogues and two other interesting compounds (**36** and **38**), to investigate whether they are substrates for the Pgp efflux pump, by determining their MDR ratios in two different epithelial cell lines overexpressing human Pgp. Simultaneously, we performed molecular docking studies of our new series of STLC-like compounds to explain the structure−activity relationship of these compounds. We also solved the crystal structures of Eg5 in complex with compounds **25** and **33** to 2.6 and 2.2 Å, respectively, and describe the important interactions between the ligands and Eg5. The results will be discussed in the context of future structure-guided drug design.

RESULTS AND DISCUSSION

Chemistry. Condensation of Ph_2C(aryl or alkyl)OH (aryl = 4-(cyclohexyl)-Ph, 4-(Ph)-Ph, 4-(*tert*-Bu)-Ph, 4-(*n*-Bu)-Ph, 4-(*i*-Pr)-Ph, 4-(*n*-Pr)-Ph, 4-(CF_3)-Ph, 4-(Et)-Ph, 4-(MeS)-Ph, 4-I-Ph, or alkyl = butan-2-yl, pentan-3-yl) **3**−**12** and **31**−**32** with L-cysteine (**13**) in the presence of $BF_3 \cdot Et_2O$ afforded target compounds **14**−**23** and **33**−**34** in 20−40% yield (Scheme 1).[18,19] Starting alcohols **3**−**12** and **31**−**32** were prepared, according to the literature,[20] in 49−95% yield by addition of phenylmagnesium bromide to the corresponding ester (data not shown). *N*,*N*-Dimethylation of STLC (**1**) was performed in the presence of formaldehyde and sodium triacetoxyborohydride to give **37** in 19% yield (Scheme 1).[22]

Inhibition of the Basal and MT-Stimulated Eg5 ATPase Activities. To further extend our knowledge of *para*-substituted STLC analogues in vitro, we determined the inhibition of the basal and the MT-stimulated Eg5 ATPase activities (Table 1). We employed an improved protocol to determine the apparent K_i values for tight binding inhibitors,[21] as described in the Experimental Section. STLC **1** and STDC **2** (*S*-trityl-D-cysteine) served as controls. The inhibition values (K_i^{app} or IC_{50}) for both the basal and MT-stimulated ATPase activities, grouped according to potency, are consistent.

When inhibiting the basal Eg5 ATPase activity, compounds with sterically demanding or polar functional groups, such as cyclohexyl, phenyl, and carboxylic acid (**14**−**15**, **28**), are weak inhibitors of Eg5 with apparent K_i values in the lower micromolar range (1.3−3.3 μM). The *tert*- and *n*-butyl analogues **16**−**17** are considerably more potent, with K_i^{app} values between 84.2 and 428.6 nM. Analogues with shorter alkyl substituents (**18**−**19**, **21**, and **26**), halogenated substitutions (**20** and **23**−**25**) and thioether/ether groups (**22** and **27**) all have apparent K_i estimates below 50 nM. For these potent compounds, the assay based on the inhibition of the basal ATPase activity is no longer suitable because the assays are performed at an Eg5 concentration of 100 nM. Instead, the IC_{50} values obtained for the inhibition of the MT-stimulated Eg5 ATPase activity (performed in the presence of 10 nM Eg5) are more reliable as the assay is closer to physiological conditions.

We then investigated the potency of four diphenylalkyl analogues (Table 2). Compounds **29**, **30**, **33**, and **34** have K_i^{app} values of <50, 174.5, 76.2, and 302.1 nM, respectively, thus, confirming the trend that the triphenyl group is not essential for effective inhibition of Eg5. This finding opens a new avenue for further SAR on the third phenyl ring. Next, we investigated two compounds, where one phenyl ring is substituted by a 2-thienyl or a 2-naphthyl moiety (**35**−**36**). While **35** is almost inactive (K_i^{app} = 58 μM), compound **36** is a very potent inhibitor of Eg5 with a K_i^{app} value <50 nM for the inhibition of the basal ATPase activity and with an IC_{50} value of 16.3 nM for the inhibition of the MT-stimulated ATPase activity.

To confirm the importance of the primary amino group, we prepared the tertiary amine **37** in which the two hydrogen atoms are substituted with methyl groups (Table 2). This compound

dx.doi.org/10.1021/jm100991m |*J. Med. Chem.* 2011, 54, 1576–1586

Table 1. K_i^{app} Values for the Inhibition of the Basal Eg5 ATPase Activity and IC_{50} Values for the Inhibition of the MT-Stimulated ATPase Activity for Novel *para*-Substituted STLC Analogues

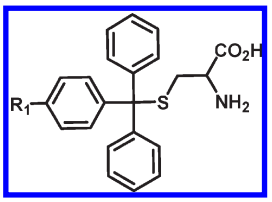

compd	R_1	inhibition of basal ATPase activity K_i^{app} (nM)	inhibition of MT-stimulated ATPase activity IC_{50} (nM)
1 (STLC)[a]	H	71.9	284.9 ± 13.7
2 (STDC)[b]	H	98.6	306.2 ± 14.2
14[a,c]	cyclohexyl	3263.7	1578 ± 277
15[a,c]	Ph	1349.7	1970 ± 469
16[a]	*tert*-Bu	428.6	1244 ± 158
17[a]	*n*-Bu	84.2	93.3 ± 5.8
18[a]	*i*-Pr	<50.0	144.0 ± 3.0
19[a]	*n*-Pr	<50.0	85.9 ± 3.2
20[a]	CF_3	<50.0	116.4 ± 5.9
21[a]	Et	<50.0	55.4 ± 0.8
22[a]	SMe	<50.0	21.8 ± 1.5
23[a]	I	<50.0	19.3 ± 2.4
24[a]	Br	<50.0	26.8 ± 0.9
25[a]	Cl	<50.0	53.3 ± 1.5
26[a]	Me	<50.0	61.7 ± 1.6
27[a]	OMe	<50.0	28.5 ± 0.9
28[c]	CO_2H	2536.3	14100 ± 2600

[a] Compounds with *R*-configuration. [b] Compound with *S*-configuration. [c] Compound is not a tight-binding inhibitor anymore.

Table 2. K_i^{app} Values for the Inhibition of the Basal Eg5 ATPase Activity and IC_{50} Values for the Inhibition of the MT-Stimulated ATPase Activity for STLC Analogues

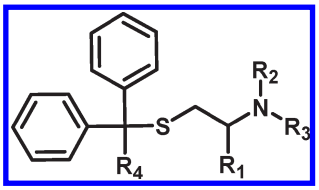

compd	R_1	R_2/R_3	R_4	inhibition of basal ATPase activity K_i^{app} (nM)	inhibition of MT-stimulated ATPase activity IC_{50} (nM)
29[a]	CO_2H	H	*n*-Bu	<50	318.8 ± 13.7
30[a]	CO_2H	H	*i*-Pr	174.5	1152.6 ± 168.2
33[a,b]	CO_2H	H	−CH(Me)Et	76.2	548.9 ± 130.0
34[a]	CO_2H	H	$-CH(Et)_2$	302.1	1634.3 ± 393.0
35[a]	CO_2H	H	2-thienyl	58333	41700 ± 21500
36[a]	CO_2H	H	2-naphthyl	<50	16.3 ± 0.5
37[a]	CO_2H	Me	Ph	ni	ni
38	H	H	Ph	156.1	395.61 ± 114.7

[a] Compounds with *R*-configuration. [b] Compound is a mixture of diastereoisomers; ni = no inhibition.

does not inhibit Eg5 activity anymore. Conversely, compound **38**, which lacks the carboxyl group, is about 30% less active than STLC. Overall, the results from the inhibition of the MT-stimulated Eg5 ATPase activity follow the same trend as observed for the inhibition of the basal Eg5 ATPase activity. The four most potent *para*-substituted analogues tested were compounds **22**, **23**, **24**, and **27**, with IC_{50} values ranging from 19.3 to 28.5 nM. Subsequently, we chose a set of representative *para*-substituted compounds and two other interesting compounds (**36** and **38**) for further evaluation in cell-based assays and MDR tumor cell lines.

dx.doi.org/10.1021/jm100991m |*J. Med. Chem.* 2011, 54, 1576–1586

Table 3. Data Collection and Refinement Statistics for Eg5−25 and Eg5−33 Complexes

	Eg5−25[a]	Eg5−33[a]
unit cell dimensions a, b, c, γ (Å, deg)	96.8, 96.8, 124.8, 120	96.35, 96.35, 124.40, 120
space group	$P3_2$	$P3_2$
beamline/detector	I03/ADSC Q315R	ID29/ADSC Q315R
molecules per asymmetric unit	3	3
resolution range (Å)	30−2.6	30.0−2.2
no. of unique reflections	40212 (5893)	65550 (9596)
completeness (%)	99.9 (100.0)[b]	99.9 (100.0)[b]
multiplicity	6.3 (6.4)	6.3 (6.3)
R_{sym} (%)	8.7 (41.1)	8.6 (28.7)
$I/\sigma(I)$	14.2 (4.8)	14.3 (6.0)
Wilson B (Å^2)/DPI[c] (Å)	57.22/0.30	33.41/0.19
Refinement Statistics		
R_{work}/R_{free} (%)	18.14/25.71	17.44/22.38
average *B* factors		
overall	40.88	34.87
main chain/side chain	39.33/42.29	33.12/36.32
no. of. ADP/inhibitor/water	3/3/377	3/3/783
rmsd in bond length[d] (Å)	0.0129	0.0130
rmsd in bond angle (deg)	1.832	1.678

[a] The *R*-enantiomer and the diastereoisomeric mixture were used for crystallization of the Eg5−**25** and Eg5−**33** complexes, respectively. [b] Values in parentheses pertain to the highest resolution shell. [c] DPI: diffraction-component precision index.[42] [d] rmsd is the root-mean-square deviation from ideal geometry.

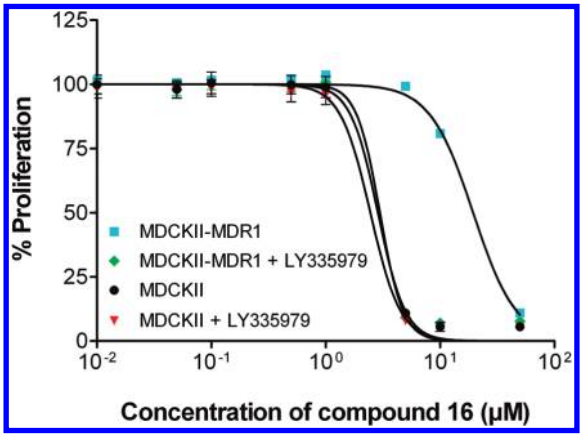

Figure 1. Growth inhibition assay using compound **16** in the MDCKII cell system in the presence and absence of the specific Pgp inhibitor LY335979. Each data point represents mean ± standard deviation for n = 24.

Growth Inhibition Assays and MDR Ratios. Growth inhibition assays were conducted in two parental cell lines (MDCKII and LLC-PK1) and then compared with the corresponding cell lines overexpressing Pgp (MDCKII-MDR1 and L-MDR1) to assess the efficiency of all compounds in the presence of Pgp-induced MDR. An example of the data is shown in Figure 1 for compound **16**. The four most active compounds in cell-based assays are **22**, **23**, **26**, and **36** with GI_{50} values between 60 and 110 nM. The most potent compounds in the LLC system were **21**, **22**, **23**, and **36**, which is similar to the results for the MDCKII system. However, they had higher GI_{50} values: between 160 and 340 nM (Table 5). These results show that STLC and its analogues are potent inhibitors of Eg5 in vitro as well as in cell-based assays and that differences observed in the extent of inhibition could originate at least in part from differences in the Eg5 primary protein sequence in porcine and canine, compared to the human protein.

A hallmark of Pgp is its capacity to accept a wide range of structurally diverse chemical compounds as substrates. Thus, defining a Pgp substrate is quite complex. As STLC exhibits the characteristics of a typical Pgp substrate: its 3 phenyl rings cause it to be lipophilic, it has a basic amino group, and it forms three hydrogen bond interactions with residues of the Eg5 inhibitor binding pocket,[22] we decided to investigate whether STLC and its *para*-substituted analogues are substrates for the Pgp efflux pumps by determining their MDR ratios.

Pgp overexpressing cells were more resistant for all *para*-substituted compounds tested than their parental counterparts, leading to MDR ratios (GI_{50} in MDR cells/GI_{50} in parental cells) above 1.0, thus indicating transport of the compounds by Pgp. Moreover, treatment of the cells with the specific Pgp inhibitor LY335979 had no significant effects on the parental cell lines but abolished MDR in the Pgp overexpressing cell lines. This restored efficiency of the compounds in the presence of the specific Pgp inhibitor confirming that the resistance can be attributed to Pgp.

The control compound vincristine, a well-known cytostatic Pgp substrate, reached the highest MDR ratio in both cell lines. In the MDCKII cell system, the MDR ratio of all STLC analogues lie between 2.0 and 6.8 with a mean of 3.2 compared to 40.3 for vincristine (Table 4). In the LLC system, where compounds have a generally higher MDR ratios than in the MDCKII system, the MDR ratios lie between 2.1 and 39.1 (mean: 20.5) compared to 70 for vincristine (Table 5). The difference in MDR ratios depend on the cell system used: MDCK cells overexpress Pgp about 500-fold, while LCC cells overexpress Pgp about 25000-fold. This is further demonstrated in taxol resistant LNCaP cells from prostate, which overexpress

Table 4. Compounds Tested for Multidrug Resistance in Matched MDCKII Cells Lines in the Absence and Presence of the Pgp Inhibitor LY335979[a]

compd	MDCKII GI_{50} (μM)	MDCKII-MDR1 GI_{50} (μM)	MDCKII + LY335979 GI_{50} (μM)	MDCKII-MDR1 + LY335979 GI_{50} (μM)	MDR ratio
vincristine	2.65 ± 0.20	106.59 ± 10.0	0.43 ± 0.05	0.34 ± 0.10	40.3
1	0.86 ± 0.15	2.30 ± 0.45	0.89 ± 0.03	0.58 ± 0.02	2.7
2	0.61 ± 0.05	3.15 ± 0.18	0.92 ± 0.06	0.78 ± 0.02	5.2
14	24.34 ± 6.10	50.76 ± 5.83	17.57 ± 1.50	17.86 ± 2.94	2.1
15	22.67 ± 5.53	68.49 ± 17.53	19.98 ± 0.81	24.53 ± 4.95	3.0
16	2.86 ± 0.26	19.51 ± 1.56	2.48 ± 0.16	3.01 ± 0.13	6.8
18	0.78 ± 0.12	2.75 ± 0.80	0.84 ± 0.02	0.88 ± 0.04	3.5
19	0.68 ± 0.07	1.68 ± 0.29	0.71 ± 0.05	0.63 ± 0.38	2.5
20	0.32 ± 0.03	0.67 ± 0.04	0.33 ± 0.02	0.27 ± 0.04	2.1
21	0.23 ± 0.06	0.56 ± 0.10	0.29 ± 0.02	0.17 ± 0.01	2.4
22	0.11 ± 0.01	0.41 ± 0.11	0.11 ± 0.01	0.21 ± 0.01	3.7
23	0.10 ± 0.01	0.33 ± 0.01	0.11 ± 0.01	0.18 ± 0.02	3.4
24	0.25 ± 0.03	0.67 ± 0.14	0.25 ± 0.01	0.21 ± 0.01	2.7
25	0.28 ± 0.03	0.56 ± 0.07	0.33 ± 0.01	0.27 ± 0.01	2.0
26	0.09 ± 0.01	0.35 ± 0.004	0.08 ± 0.01	0.12 ± 0.01	3.8
27	0.22 ± 0.01	0.54 ± 0.13	0.24 ± 0.03	0.08 ± 0.01	2.5
36	0.06 ± 0.01	0.19 ± 0.002	0.07 ± 0.01	0.05 ± 0.01	3.1
38	0.74 ± 0.05	0.57 ± 0.07	0.85 ± 0.03	0.61 ± 0.01	0.8

[a] Statistical analysis was conducted using analysis of variance (ANOVA) with Bonferroni's multiple comparison post hoc test. For all compounds investigated, there was a statistically significant difference between GI_{50} in MDCKII and MDCKII-MDR1 cells ($p < 0.001$). There was no statistically significant difference between GI_{50} in MDCKII cells without LY335979 and MDCKII or MDCKII-MDR cells with LY335979 treatment.

Table 5. Compounds Tested for Multidrug Resistance in Matched LLC-PK1 Cell Lines in the Absence and Presence of the Pgp Inhibitor LY3359790[a]

compd	LLC-PK1 GI_{50} (μM)	L-MDR1 GI_{50} (μM)	LLC-PK1 + LY335979 GI_{50} (μM)	L-MDR1 + LY335979 GI_{50} (μM)	MDR ratio
vincristine	0.03 ± 0.02	21. ± 0.5	nt	nt	70[b]
1	1.06 ± 0.15	32.99 ± 11.73	1.11 ± 0.09	3.02 ± 0.66	31.0
2	0.94 ± 0.05	36.58 ± 13.71	1.07 ± 0.13	4.46 ± 0.20	39.1
14	47.90 ± 3.17	nd	64.94 ± 1.11	56.85 ± 2.67	nd
15	77.85 ± 1.48	nd	75.56 ± 23.07	109.88 ± 18.33	nd
16	4.28 ± 0.22	nd	5.41 ± 0.71	13.5 ± 5.6	>12.5
18	1.05 ± 0.05	36.69 ± 7.03	1.51 ± 0.26	1.05 ± 0.13	34.8
19	1.95 ± 0.23	37.64 ± 8.03	1.10 ± 0.62	1.76 ± 0.58	19.3
20	1.00 ± 0.03	8.02 ± 2.65	0.51 ± 0.04	1.02 ± 0.02	8.0
21	0.34 ± 0.01	10.85 ± 0.91	0.30 ± 0.03	0.16 ± 0.02	31.8
22	0.34 ± 0.06	11.85 ± 4.60	0.30 ± 0.01	0.67 ± 0.06	35.1
23	0.33 ± 0.16	9.17 ± 1.58	0.44 ± 0.02	0.61 ± 0.06	27.6
24	3.20 ± 0.63	6.78 ± 0.19	2.12 ± 0.80	2.35 ± 1.01	2.1
25	2.11 ± 0.19	6.21 ± 1.75	2.45 ± 0.60	1.61 ± 0.18	2.9
26	1.05 ± 0.01	3.83 ± 0.39	1.18 ± 0.28	0.49 ± 0.12	3.7
27	1.66 ± 0.27	6.91 ± 0.29	2.05 ± 0.60	1.65 ± 0.15	4.2
36	0.16 ± 0.05	6.18 ± 0.89	0.18 ± 0.02	0.29 ± 0.01	38.6
38	3.29 ± 0.74	4.83 ± 1.17	3.88 ± 0.23	4.81 ± 2.16	1.5

[a] Statistical analysis was conducted using analysis of variance (ANOVA) with Bonferroni's multiple comparison post hoc test. For all compounds investigated, there was a statistically significant difference between GI_{50} in LLC-PK1 and L-MDR1 cells ($p < 0.01$ for compounds **2**, **22**, and **24**−**25**, and $p < 0.001$ for all other compounds). There was no statistically significant difference between GI_{50} in LLC-PK1 cells without LY335979 and LLC-PK1 or L-MDR1 cells with LY335979 treatment. [b] Data for vincristine were published previously (Peters et al., 2006). nt, not tested; nd, not determined.

Pgp by only 8.8-fold. The MDR ratio for STLC is 1; thus, indicating that in this cell type, STLC is not a substrate for Pgp at all.[23]

Nonetheless, these results show that most of the STLC analogues investigated are, albeit weak, Pgp substrates and thus have the potential to overcome multidrug resistance. It is interesting to note that in the LLC cell system, STLC, STDC, and analogues with more bulky *para*-substituents show an MDR ratio of about 30, whereas less structurally demanding compounds (Cl, Br, Me, and OMe *para*-substituents) have MDR

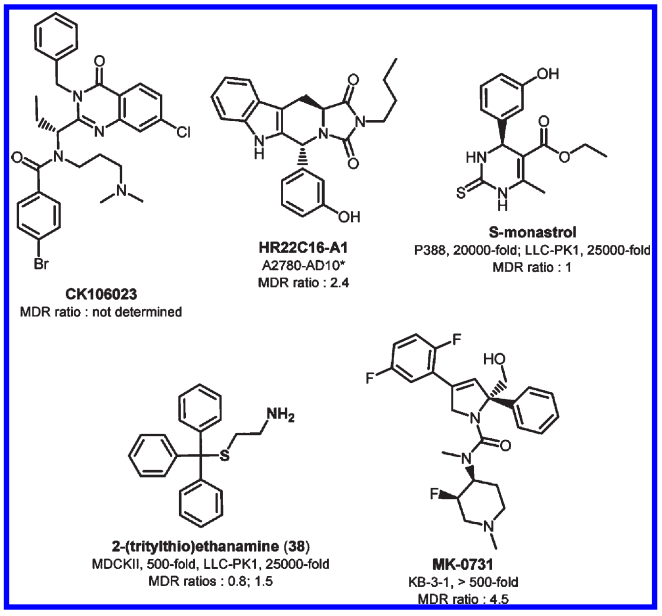

Figure 2. Chemical structure and names (in bold) of Eg5 inhibitors that have been tested in the stated cell lines, with reported upregulation of Pgp mRNA, for their susceptibility to the human and mouse ABC transporter, Pgp. *Overexpression level of Pgp mRNA not reported.

ratios below 4.2. MDR data for only a few Eg5 inhibitors have been reported so far (Figure 2),[17,24−28] but Cox et al. consider compounds with MDR ratios of less than 10 as having the potential to overcome MDR.[27,28] As the results from the LLC cell system divides the STLC analogues into two groups, those with MDR ratios about 20−40 and those with MDR ratios less than 10, we will therefore concentrate future work on the latter.

It is also known that some MDR transporters possess stereoselectivity: only one of the enantiomers of a compound is a substrate for the transporter.[4] We therefore examined whether Pgp has enantioselectivity for the two enantiomers STLC and STDC. However, the MDR ratios of 2.7 and 5.2 measured for STLC and STDC in the MDCK cell system and of 31.0 and 39.1 in the LLC cell system indicate that there is no significant stereoselectivity of Pgp between the two enantiomers.

Finally, we decided to determine the MDR ratio of compound **38**, which lacks the carboxyl group that forms hydrogen bond interactions with Arg221 and several structural water molecules in its vicinity. To our surprise, it has MDR ratios of 0.8 and 1.5 in the MDCKII and LLC-PK1 cell systems, respectively, and is clearly not a substrate for Pgp.

Docking of Compounds 1−2, 14−28, and 36 into the New Eg5−STLC Complex. We used the docking program GOLD[29] to perform molecular docking studies of the analogues described in Table 1 to explain the structure−activity relationship of compounds **1**−**2**, **14**−**28**, and **36**. First, we compared our experimentally obtained conformation of STLC[22] with the highest scored docking pose of STLC that had been prepared for a previous paper[17] (Figure 3A). As described in that paper, the docking of STLC was performed in the binding site of a different complex (PDB code: 2FME). To keep the ligands' relative orientations within their binding sites, we aligned them by overlaying the α carbon atoms of their respective binding site amino acids. As can be seen from the figure, our predictions were highly accurate, with an rms deviation of 0.232 Å between the experimental and docked poses.

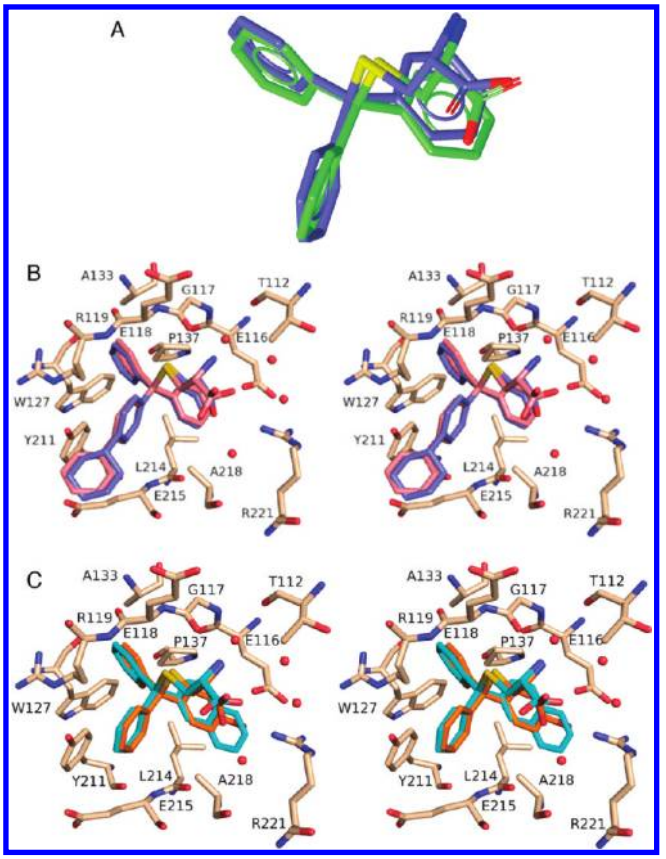

Figure 3. Comparison of experimental conformation with docked pose of STLC and proposed docking poses for a selection of interesting *para*-substituted analogues. (A) Overlay of STLC previously docked into PDB structure 2FME[17] (blue) and STLC obtained by X-ray crystallography[22] (green). Structural overlay was performed in LigandScout[41] via alignment of the α carbon atoms of the corresponding protein binding sites. (B) Stereo plot showing compounds **14** (purple) and **15** (pink) docked into the Eg5−STLC complex (PBD code: 2WOG),[22] with the *para*-substituent pointing toward the solvent. (C) Stereo plot showing compounds **24** (orange) and **36** (light blue) docked into the Eg5−STLC complex (PBD code: 2WOG),[22] with the *para*-substituent pointing toward the core of the protein.

For the protein template, we chose the binding site in chain A of the Eg5−STLC complex (PDB code: 2WOG). The results are highly similar to the ones obtained in our previous studies: all highly ranked conformations show the same interactions between the protein and the ligands' amino and the carboxylic groups (except for **2** (data not shown)) as compared to what is observed in the experimental Eg5−STLC and Eg5−**33** complexes. In the complex of Eg5 with compound **2**, which is the *R*-enantiomer of **1**, the carboxylic group points outward and interacts only with water molecules, while the rest of the molecule remains in an orientation similar to the other poses. The three phenyl rings of all compounds are placed into the same hydrophobic regions that were observed in the crystal structures, leaving only the placement of the *para*-substituent as a point of possible variation.

With the exception of the bulkier cyclohexyl and phenyl substituents (**14**−**15**), which point toward the solvent (pocket 1; Figure 3B), *para*-substituents were preferentially placed in the pocket formed by Ile136, Pro137, Leu160, Leu214, Phe239, and the salt bridge between Glu116 and Arg221 (pocket 3;

Figure 3C). For the smaller substituents, for example compounds **20**−**27**, the additional hydrophobic interaction might be the reason for increased inhibition. Together, the docking and structural studies reveal that the hydrophobic interaction of the smaller substituents with the core of the protein may be the reason for increased inhibition, whereas compounds with larger substituents have lower affinities because of steric hindrance. The decreased inhibition by **28** is explained by the placement of its polar carboxylate group within a mainly hydrophobic environment. For **14** and **15**, the *para*-substituents stick out into the solvent (beyond pocket 1), adding no beneficial interactions along the protein surface. It is noteworthy that not a single *para*-substituent was placed in pocket 2.

Comparison of Eg5−STLC, Eg5−25, and Eg5−33 Crystal Structures. Previously, we determined the structure of Eg5 in complex with STLC to understand the interactions of the ligand with Eg5 at the inhibitor-binding pocket.[22] The Eg5−STLC structure revealed not only the final inhibitor-bound state of Eg5 but also an unprecedented intermediate state, whereby local changes at the inhibitor-binding pocket have not propagated to structural changes at the switch II cluster and neck-linker. We also identified several important hydrogen bond interactions between Eg5 and the cysteine moiety of STLC that contribute to the tight binding of the inhibitor. These interactions are also observed in another Eg5−STLC structure (PDB code: 3KEN) by Kim et al.[30] The three phenyl rings of STLC are buried in the mostly hydrophobic part of the inhibitor-binding pocket. As free rotation is possible around the C−S bond, the three phenyl rings can interchange positions in the hydrophobic pocket. Hence, it is difficult to determine which phenyl ring to modify in order to increase the potency of the inhibitor. As such, we set out to determine the structures of Eg5 in complex with **25**, where one of the phenyl rings has a *para*-substituted chlorine, and **33**, where one of the phenyl rings has been substituted by an alkyl chain, resulting in a diastereoisomeric analogue.

We determined the crystal structures of Eg5 in complex with **25** and **33** to a resolution of 2.6 and 2.2 Å, respectively. Data collection and refinement statistics are presented in Table 3. Both the Eg5−**25** and Eg5−**33** complexes crystallize in space group $P3_2$ with 3 molecules per asymmetric unit. Two of the molecules in the asymmetric unit reveal the final inhibitor-bound state of Eg5, whereby Loop L5 has swung downward to close the inhibitor-binding pocket, the switch II cluster has moved upward, and the neck-linker has adopted a docked conformation. The third molecule in the asymmetric unit, however, revealed an intermediate state identical to that observed with the Eg5−STLC structure.[22] This intermediate state provides structural evidence for the sequence of drug-induced conformational changes.

Although we used the diastereoisomeric mixture of **33** for crystallization of the Eg5−inhibitor complex, we fitted only one of the diastereoisomers, *S*-(2-methyl-1,1-diphenylbutyl)-L-cysteine, into the structure. Upon analyzing the inhibitor-binding pocket, we observed identical hydrogen bond interactions between Eg5 and the cysteine moieties of STLC, **25** and **33** (Figure 4C). In addition, **33** appeared to form one more hydrogen bond with water, as compared to STLC and **25**. This hydrogen bond, formed between an oxygen (OXT) of the carboxyl group of the cysteine moiety and a structural water molecule, is only observed in molecules A and B of the Eg5−**33** structure.

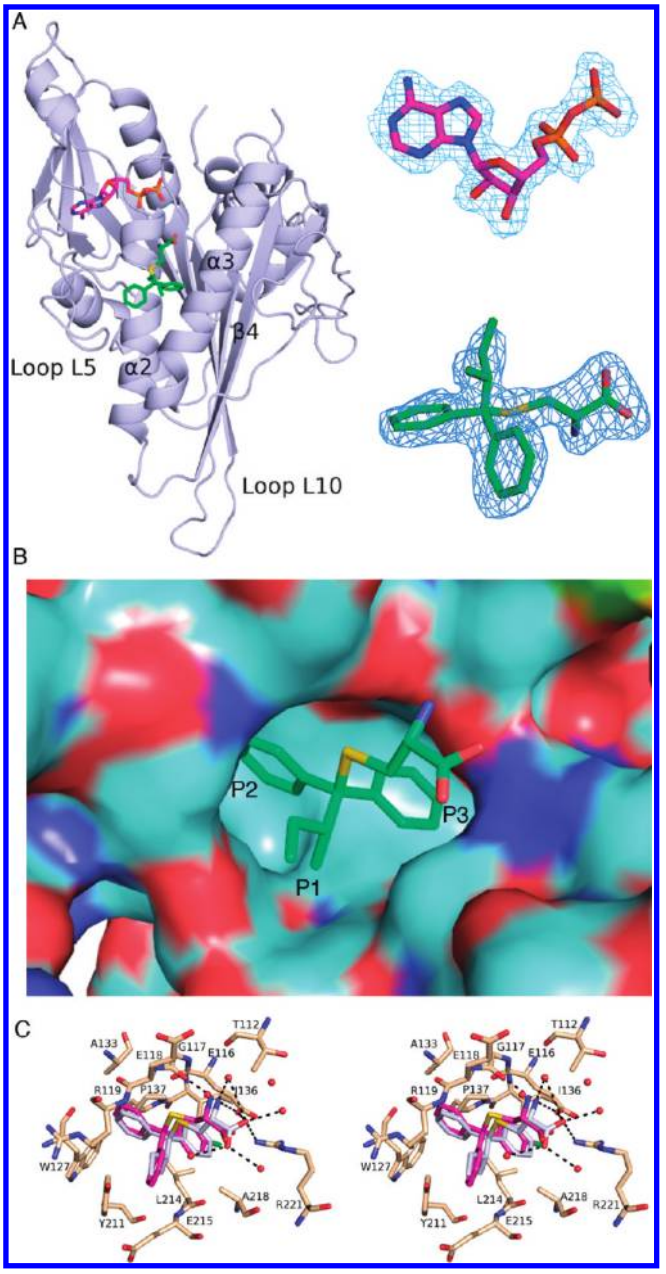

Figure 4. (A) Overall ternary structure of the Eg5 motor domain in complex with Mg^{2+}ADP (red) and compound **33** (green) as ball-and-stick models. Molecule B was used to generate this figure. Right: difference map ($2F_o - F_c$) (contoured at $\sigma = 1.00$, colored in blue) for ADP in the catalytic site and omit map ($F_o - F_c$) (contoured at $\sigma = 3.00$, colored in blue) for **33** bound in the inhibitor-binding pocket. (B) Surface diagram showing the positions of the two phenyl rings and the *tert*-butyl group of compound **33** (PDB code: 2X2R) in the respective pockets, numbered P1, P2, and P3. (C) Stereo plot showing compound **33** (gray) in the inhibitor-binding pocket and important hydrophobic, aromatic, and hydrogen bond (represented by broken lines) interactions (within 4 Å) between **33** and the Eg5 main chain and side chain molecules and structural water molecules, which are represented by red spheres. Compound **25** (magenta) is overlaid to show the position of the *para*-substituted chlorine (green) on one of the phenyl rings in subpocket P3.

With a high-resolution structure and well-defined electron density map (Figure 4A), we were able to determine undoubtedly the location of the *para*-substituted chlorine and the alkyl

chain substituent of **25** and **33**, respectively. The chlorine *para*-substituted phenyl ring is buried in the pocket formed by Ile136, Pro137, Leu160, Leu214, Phe239, and the salt bridge between Glu116 and Arg221, while the alkyl chain points toward the solvent-exposed region of the protein (Figure 4B) and the methyl group (CAA) forms a C−H−π interaction with the phenyl ring of Tyr211 (Figure 4C). The substitution of the phenyl ring by the alkyl chain could be the main reason for the slight decrease in potency of **33** compared to STLC, which has an additional offset stacked $\pi-\pi$ interaction between the second phenyl group and Tyr211 (Figure 4C). In short, the crystal structures of Eg5−**25** and Eg5−**33** validate the above docking studies and provide insight into the arrangement of the substituents about the carbon CAX and may aid subsequent structure-based drug design.

CONCLUSIONS

The antitumor effects of STLC and related compounds have first been described in the early 1970s in murine leukemia in vivo.[18,31,32] In the early 1990s, STLC was classified as an antimitotic agent that does not target tubulin/MTs, but the protein target remained unknown.[33] Previously, we identified human Eg5 as the major target for STLC,[12] investigated the effect of the inhibitor in vitro,[14,34] pinpointed its binding region on Eg5,[35,36] and described the effect of STLC in cell-based assays, namely the induction of mitotic arrest and subsequent cell death in HeLa cells.[14]

In an effort to improve the efficiency of the inhibitor, two laboratories conducted initial SAR studies, which led to the identification of more potent STLC derivatives.[16,17] We have since synthesized a new series of *para*-substituted STLC analogues. Investigation of the inhibition of basal and MT-stimulated Eg5 ATPase activities reveals that compounds with sterically less demanding *para*-substituents are generally more potent than those with bulkier *para*-substituents. This result is reinforced by the cell-based assays in two different cell lines. Furthermore, using cell lines overexpressing Pgp, we showed that STLC and its analogues are weak substrates of Pgp when compared with vincristine. In addition, compounds with less sterically demanding substituents generally have lower MDR ratios, thus suggesting that they may have greater potential in overcoming susceptibility to the Pgp efflux pump.

To understand at the atomic level why sterically less demanding substituents are more potent, we performed docking studies to study the structure−activity relationship of the compounds. The results show that the sterically less demanding substituents point toward the core of the protein, while the bulkier substituents generally fit into the solvent-exposed subpocket. We also determined the structures of two new Eg5−inhibitor complexes, which corroborate the docking results. Together, the docking and structural studies reveal that the hydrophobic interaction of the smaller substituents with the core of the protein may be the reason for increased inhibition, while that of the larger substituents is lost due to steric hindrance.

EXPERIMENTAL SECTION

Chemistry. *General Methods.* Melting points were determined using a Büchi capillary instrument and are uncorrected. Optical rotations were measured at the sodium D line (589 nm) at 25 °C with a Perkin-Elmer 241 polarimeter using a 1 dm path length cell. ^{1}H spectra were recorded on a Bruker Advance 300 MHz spectrometer. Chemical shifts are reported in ppm (δ) relative to tetramethylsilane as an internal standard. Mass spectra were recorded with a Perkin-Elmer SCIEX API spectrometer. Elemental analyses were performed on a Thermoquest Flash 1112 series EA analyzer. Elemental analyses were found to be within ±0.4 of the theorical values. Purity of tested compounds was >95%. All commercially available reagents and solvents were used without further purification. Compounds **1**−**2**, **24**−**28**, and **35**−**36** were obtained from the Drug Synthesis and Chemistry Branch, Developmental Therapeutics Program, Division of Cancer Treatment and Diagnosis, National Cancer Institute, USA. The identity of the NCI compounds was confirmed by Liquid chromatography−mass spectrometry and NMR. Alcohols **3**−**12** and **31**−**32** and compounds **29** and **30** were prepared according to the literature.[16,19] The other compounds were synthesized as follows. The synthesis and spectroscopic details for a few key compounds (**18**−**23** and **33**) are shown below, while the rest are in the Supporting Information.

*General Procedure for Preparation of Compounds **18**−**23** and **33**.* At 0 °C and under argon atmosphere, a solution of $BF_3 \cdot Et_2O$ (1.33 mmol) was added dropwise to a solution of appropriate alcohol (0.86 mmol), L-cysteine (**13**) (0.77 mmol) in AcOH (1 mL). The reaction mixture was stirred at room temperature for 2 h. Addition of a 10% NaOAc solution (2 mL), then H_2O (2 mL) led to the formation of a gum. After elimination of the supernatant, the final compound was precipitated by addition of Et_2O or Et_2O/MeOH (9:1 to 1:1). The desired compounds **18**−**23** and **33** were obtained by filtration in the range of 20−40% yield.

S-(1,1-Diphenyl[4-(isopropyl)phenyl]methyl)-L-cysteine (18). Starting alcohol = (4-isopropylphenyl)diphenylmethanol. Yield 31%; mp 168−169 °C. $[\alpha]_{589}^{25}$ = +52 (*c* 0.51, MeOH). ^{1}H NMR (300 MHz, $CD_3OD + D_2O$): δ 1.24 (d, 6H, *J* = 7.0 Hz, 2 CH_3), 2.68 (dd, 1H, *J* = 9.2, 13.4 Hz, CH_2), 2.82 (dd, 1H, *J* = 4.1, 13.4 Hz, CH_2), 2.88 (sept, *J* = 7.0 Hz, CH), 3.01 (dd, 1H, *J* = 4.1, 9.2 Hz, CH), 7.17−7.46 (m, 14H, H_{Ar}). MS (ESI): *m*/*z* 428 $(M + Na)^+$. Anal. ($C_{25}H_{27}NO_2S$) C, H, N.

S-(1,1-Diphenyl[4-(propyl)phenyl]methyl)-L-cysteine (19). Starting alcohol = (4-propylphenyl)diphenylmethanol. Yield 40%; mp 142−144 °C. $[\alpha]_{589}^{25}$ = +60 (*c* 0.51, MeOH). ^{1}H NMR (300 MHz, $CD_3OD + D_2O$): δ 0.94 (t, 3H, *J* = 7.6 Hz, CH_3), 1.63 (sex, 2H, *J* = 7.6 Hz, CH_2), 2.57 (broad t, 2H, *J* = 7.6 Hz, CH_2), 2.68 (dd, 1H, *J* = 9.2, 13.4 Hz, CH_2), 2.82 (dd, 1H, *J* = 4.1, 13.4 Hz,CH_2), 3.02 (dd, 1H, *J* = 4.1, 9.2 Hz, CH), 7.12−7.46 (m, 14H, H_{Ar}). MS (ESI): *m*/*z* 428 $(M + Na)^+$. Anal. ($C_{25}H_{27}NO_2S$) C, H, N.

S-(1,1-Diphenyl[4-trifluoromethylphenyl]methyl)-L-cysteine (20). Starting alcohol = (4-trifluoromethylphenyl)diphenylmethanol. Yield 29%; mp 154−155 °C. $[\alpha]_{589}^{25}$ = +46 (*c* 0.58, MeOH). ^{1}H NMR (300 MHz, $CD_3OD + D_2O$): δ 2.70 (dd, 1H, *J* = 8.7, 13.1 Hz, CH_2), 2.81 (dd, 1H, *J* = 4.2, 13.1 Hz,CH_2), 3.18 (dd, 1H, *J* = 4.2, 8.7 Hz, CH), 7.24−7.46 (m, 12H, H_{Ar}), 7.62 (broad d, 2H, *J* = 8.8 Hz, H_{Ar}), 7.68 (broad d, 2H, *J* = 8.8 Hz, H_{Ar}). MS (ESI): *m*/*z* 454 $(M + Na)^+$. HRMS (ESI) calculated for $C_{23}H_{20}F_3NNaO_2S$ 454.1064; found 454.1066.

S-(1,1-Diphenyl[4-(ethyl)phenyl]methyl)-L-cysteine (21). Starting alcohol = (4-ethylphenyl)diphenylmethanol. Yield 25%; mp 153−154 °C. $[\alpha]_{589}^{25}$ = +62 (*c* 0.53, MeOH). ^{1}H NMR (300 MHz, $CD_3OD + D_2O$): δ 1.22 (t, 3H, *J* = 7.6 Hz, CH_3), 2.63 (q, 2H, *J* = 7.6 Hz, CH_2), 2.70 (dd, 1H, *J* = 9.2, 13.4 Hz, CH_2), 2.82 (dd, 1H, *J* = 4.0, 13.4 Hz, CH_2), 3.02 (dd, 1H, *J* = 4.0, 9.2 Hz, CH), 7.14−7.46 (m, 14H, H_{Ar}). MS (ESI): *m*/*z* 414 $(M + Na)^+$. Anal. ($C_{24}H_{25}NO_2S$) C, H, N.

S-(1,1-Diphenyl[4-thiomethylphenyl]methyl)-L-cysteine (22). Starting alcohol = (4-thiomethylphenyl)diphenylmethanol. Yield 33%; mp 155−156 °C. $[\alpha]_{589}^{25}$ = +58 (*c* 0.51, MeOH). ^{1}H NMR (300 MHz, $CD_3OD + D_2O$): δ 2.49 (s, 3H, CH_3), 2.70 (dd, 1H, *J* = 9.0, 13.2 Hz, CH_2), 2.84 (dd, 1H, *J* = 4.1, 13.2 Hz, CH_2), 3.12 (dd, 1H, *J* = 4.1, 9.0 Hz, CH), 7.22−7.49 (m, 14H, H_{Ar}). MS (ESI): *m*/*z* 432 $(M + Na)^+$. Anal. ($C_{23}H_{23}NO_2S_2$) C, H, N.

S-(1,1-Diphenyl[4-iodophenyl]methyl)-L-cysteine (23). Starting alcohol = (4-iodophenyl)diphenylmethanol. Yield 20%; mp 159−160 °C. $[\alpha]_{589}^{25}$ = +47 (*c* 0.57, MeOH). ^{1}H NMR (300 MHz, CD_3OD + D_2O): δ 2.67 (dd, 1H, *J* = 9.1, 13.4 Hz, CH_2), 2.78 (dd, 1H, *J* = 4.1, 13.4 Hz, CH_2), 3.13 (dd, 1H, *J* = 4.1, 9.1 Hz, CH), 7.21−7.44 (m, 12H, H_{Ar}), 7.67 (d, 2H; *J* = 8.6 Hz, H_{Ar}). MS (ESI): *m*/*z* 512 $(M + Na)^+$. Anal. ($C_{22}H_{20}INO_2S$) C, H, N.

S-(2-Methyl-1,1-diphenylbutyl)-L-cysteine (33). Starting alcohol = 2-methyl-1,1-diphenylbutanol. Compound **33** was obtained as a diastereoisomeric mixture. Yield 35%; mp 170−171 °C. $[\alpha]_{589}^{25}$ = +16 (*c* 0.50, MeOH). ^{1}H NMR (300 MHz, CD_3OD + D_2O): δ 0.40−0.65 (m, 1H, CH_2), 0.92−1.01 (m, 6H, 2 CH_3), 1.91−2.04 (m, 1H, CH_2), 2.45−2.55 (m, 1H, CH), 2.61−2.81 (m, 3H, CH + CH_2), 7.24−7.50 (m, 10H, H_{Ar}). MS (CI): *m*/*z* 344 $(M + H)^+$. Anal. ($C_{20}H_{25}NO_2S$) C, H, N.

Biology. *Expression and Purification of Human Eg5.* The motor domain of human Eg5 (residues 1−368) was expressed and purified as previously described.[22]

Eg5 Steady-State ATPase Assays. The inhibition of the basal and MT-stimulated ATPase Eg5 activities by STLC analogues was determined using a new protocol, which differs considerably from the protocol previously described.[13,17,34] Experiments were performed in triplicate, and the data are reported as means and their standard deviations. The new protocol is based on the manuscript by Murphy et al., which provides rules for accurate measurements of the apparent K_i values for tight binding inhibitors,[21] for which the K_i^{app} can be difficult to determine accurately.[37] Therefore, we refer to our previous and new measurements as "estimates". First, we substituted the Eg5 construct $Eg5_{1-386}$ containing a C-terminal His_6-tag with untagged $Eg5_{1-368}$. The cloning, expression, and purification methods have been described previously.[22] The old Eg5 construct has a maximum activity at 300 mM NaCl,[13] whereas the new Eg5 construct can be measured at 150 mM NaCl, which is closer to physiological conditions. The inhibition of the basal ATPase activity was measured at 100 and 400 nM of Eg5, and the concentration of the inhibitor analogues used was $30[E]_T$, which corresponds to 3 and 12 μM as the highest concentrations, followed by a 1.5-fold inhibitor dilution scheme. The IC_{50} values were plotted against the Eg5 concentration, and the *y*-intercept of the plot represents the K_i^{app} value. The inhibition of the MT-stimulated ATPase activity was measured at an Eg5 concentration of 10 nM in the presence of 1 μM MTs and 1 mM Mg^{2+}ATP. The data were fitted to the following equation:

$$y = \frac{(y_{max} - y_{min})}{\left(1 + \frac{[I]}{IC_{50}}\right)} + y_{min}$$

where *y* is the fractional activity, y_{max} is the maximum value of *y* observed at zero inhibitor concentration, y_{min} represents the minimum value of *y* obtained at the highest inhibitor concentration, [I] is the inhibitor concentration, and IC_{50} is the inhibitor concentration necessary to achieve 50% inhibition of the initial enzyme activity.

Cell-Based Assays. MDCKII and MDCKII-MDR1 cells were generated and cultured as previously described.[38] LLC-PK1 and L-MDR1 cells were generated and cultured as previously described.[39] Growth inhibition assays using the above cells were carried out as previously described.[26] Each experiment was performed at least in triplicate with *n* = 8 wells for each concentration. The half-maximum growth inhibitory concentration (GI_{50}) was calculated by a standard nonlinear four-parameter fit (sigmoidal concentration−response fit) using Prism 5.0 (GraphPad Software, San Diego, CA, USA).

MDR Ratio. The MDR ratio was calculated by dividing the GI_{50} in the Pgp overexpressing cell line by the GI_{50} in the corresponding parental cell line. If a drug is transported by Pgp, cell lines with overexpression of Pgp will be more resistant to the antiproliferative effects provoked by the compound, as compared to the corresponding parental cell line, due to their ability to extrude the drug. Thus, the MDR ratio would exceed 1. In the presence of a specific Pgp inhibitor (Zosuquidar, LY335979), resistance due to the overexpression of Pgp is abrogated, thus confirming the efflux by Pgp is responsible for the observed resistance. Data are presented as mean ± standard deviation. Statistical significance of differences in the GI_{50} values were assessed using analysis of variance (ANOVA) with Bonferroni's multiple comparison test for post hoc pairwise comparison using InStat Version 3.10 (GraphPad Software, San Diego, CA, USA).

*Crystallization of the Eg5−**25** and Eg5−**33** Complex.* Purified Eg5 (20 mg/mL) was incubated with 2 mM **25** or **33** (in DMSO) for 2 h on ice. Crystals of Eg5 with **25** appeared after 1 month in hanging drops by mixing 1 μL of protein−inhibitor complex with 1 μL of reservoir solution containing 24% polyethylene glycol-3350, 0.25 M ammonium sulfate, 0.01 M trimethylamine hydrochloride, and 0.1 M MES pH 6.0 in VDX plates (Hampton Research) at 4 °C. A cuboidal crystal with dimensions of approximately 0.1 mm × 0.1 mm × 0.2 mm was immersed in cryoprotectant solution (28.8% polyethylene glycol-3350, 0.3 M ammonium sulfate, 0.012 M trimethylamine hydrochloride, 0.12 M MES pH 6.5, 0.06 M KCl, and 20% erythritol) and flash frozen in liquid nitrogen. Crystals of Eg5 with **33** appeared after 1 month in hanging drops by mixing 2.5 μL of protein−inhibitor complex with 2.5 μL of reservoir solution containing 25% polyethylene glycol-3350, 0.15 M sodium tartrate dibasic dihydrate, and 0.1 M MES pH 6.0 in VDX plates (Hampton Research) at 4 °C. A block-shaped crystal with dimensions of approximately 0.1 mm × 0.1 mm × 0.2 mm was immersed in cryoprotectant solution (24% polyethylene glycol-3350, 0.24 M sodium sulfate decahydrate, 0.12 M MES pH 6.5, 0.06 M KCl, and 20% erythritol) and flash frozen in liquid nitrogen.

Data Collection and Processing. Diffraction data for Eg5−**25** and Eg5−**33** were recorded at the Diamond Light Source (station I03) and European Synchrotron Radiation Facility (station ID29),respectively. Detailed descriptions of data processing, structure solution and refinement are found in the Supporting Information S4.

Docking. All docking calculations were performed on a PC equipped with a 2.13 GHz Core 2 Duo processor and 3 GB of RAM, running Fedora Core 8 Linux. Ligands were drawn in the protonation states that are present at physiological pH value (protonated amino groups, deprotonated carboxylic acid groups) and converted from SMILES into 3D conformations with Omega 2.2.1.[40] Binding site preparation of the Eg5−STLC complex and docking studies were performed with the GOLD Suite 1.0.1, including Gold 4.0.1 and Hermes 1.0.[29] All waters present in the binding site were allowed to be replaced by the ligand or to change their orientation. GoldScore was used for scoring function, and early termination was disabled. All other settings were kept at their default values. LigandScout v2.03 was used for visual inspection of the docked poses.[41]

■ ASSOCIATED CONTENT

Supporting Information. Elemental analyses, synthesis, and spectroscopic details for compounds **14**−**17**, **34**, and **37**, and data collection and processing material and methods. This material is available free of charge via the Internet at http://pubs.acs.org.

Accession Codes

†Coordinate and structure factor files for the Eg5−**25** and Eg5−**33** complexes (PDB ID: 2XAE (Eg5−**25**) and 2X2R (Eg5−**33**)) were deposited at the Protein Data Bank.

■ AUTHOR INFORMATION

Corresponding Author

*Phone: +44-141-330-3186. Fax: +44-141-942-6521. E-mail: f.kozielski@beatson.gla.ac.uk.

■ ACKNOWLEDGMENT

We thank David Flot of ESRF and of EMBL-Grenoble and Katherine McAuley of Diamond Light Source for assistance and support in using beamlines ID29 and I03, respectively. We also thank Anna-Lena Gund and Stephanie Rosenzweig for their excellent technical assistance with the growth inhibition assays. Kristal Kaan holds a National Science Scholarship and is financed by A*STAR, Singapore. This publication contains part of the doctoral thesis of KK. Katarzyna Tkocz held a Leonardo da Vinci Lifelong Learning Programme scholarship. We thank CR-UK for financial support.

■ ABBREVIATIONS USED

DMSO, dimethylsulfoxide; FCS, fetal calf serum; GI_{50}, half-maximum growth inhibitory concentration; IC_{50}, median inhibitory concentration; K_i^{app}, apparent inhibition constant; KSP, kinesin spindle protein; MTs, microtubules; NCI, National Cancer Institute; PDB, Protein Data Bank; STDC, *S*-trityl-D-cysteine; STLC, *S*-trityl-L-cysteine; MI_{50}, 50% mitotic index concentration; MDR, multidrug resistance; Pgp, P-glycoprotein; CENP-E, centromere-associated protein E; PLK1, polo-like kinase 1; SAR, structure−activity relationship; DMEM, Dulbecco's Modified Eagle Medium; PBS, phosphate buffered saline; ni, no inhibition; nd, not determined; nt, not tested

■ REFERENCES

(1) Jordan, M. A.; Wilson, L. Microtubules as a target for anticancer drugs. *Nature Rev. Cancer* **2004**, *4*, 253–265.

(2) Orr, G. A.; Verdier-Pinard, P.; McDaid, H.; Horwitz, S. B. Mechanisms of Taxol resistance related to microtubules. *Oncogene* **2003**, *22*, 7280–7295.

(3) Kavallaris, M. Microtubules and resistance to tubulin-binding agents. *Nature Rev. Cancer* **2010**, *10*, 194–204.

(4) Kerns, E. H.; Di, L. *Drug-Like Properties: Concepts, Structure Design and Methods. From ADME to Toxicity Optimization*. Elsevier: New York, 2008.

(5) Sarli, V.; Giannis, A. Targeting the kinesin spindle protein: basic principles and clinical implications. *Clin. Cancer Res.* **2008**, *14*, 7583–7587.

(6) Huszar, D.; Theoclitou, M. E.; Skolnik, J.; Herbst, R. Kinesin motor proteins as targets for cancer therapy. *Cancer Metastasis Rev.* **2009**, *28*, 197–208.

(7) Strebhardt, K.; Ullrich, A. Targeting polo-like kinase 1 for cancer therapy. *Nature Rev. Cancer* **2006**, *6*, 321–330.

(8) Jackson, J. R.; Patrick, D. R.; Dar, M. M.; Huang, P. S. Targeted anti-mitotic therapies: can we improve on tubulin agents?. *Nature Rev. Cancer* **2007**, *7*, 107–117.

(9) Wood, K. W.; Chua, P.; Sutton, D.; Jackson, J. R. Centromere-associated protein E: a motor that puts the brakes on the mitotic checkpoint. *Clin. Cancer Res.* **2008**, *14*, 7588–7592.

(10) Blangy, A.; Lane, H. A.; d'Herin, P.; Harper, M.; Kress, M.; Nigg, E. A. Phosphorylation by p34cdc2 regulates spindle association of human Eg5, a kinesin-related motor essential for bipolar spindle formation in vivo. *Cell* **1995**, *83*, 1159–1169.

(11) Rowinsky, E. K.; Eisenhauer, E. A.; Chaudhry, V.; Arbuck, S. G.; Donehower, R. C. Clinical toxicities encountered with paclitaxel (Taxol). *Semin. Oncol.* **1993**, *20*, 1–15.

(12) DeBonis, S.; Skoufias, D. A.; Lebeau, L.; Lopez, R.; Robin, G.; Margolis, R. L.; Wade, R. H.; Kozielski, F. In vitro screening for inhibitors of the human mitotic kinesin Eg5 with antimitotic and antitumor activities. *Mol. Cancer Ther.* **2004**, *3*, 1079–1090.

(13) Kozielski, F.; DeBonis, S.; Skoufias, D. A. Screening for inhibitors of microtubule-associated motor proteins. *Methods Mol. Med.* **2007**, *137*, 189–207.

(14) Skoufias, D. A.; DeBonis, S.; Saoudi, Y.; Lebeau, L.; Crevel, I.; Cross, R.; Wade, R. H.; Hackney, D.; Kozielski, F. *S*-Trityl-L-cysteine is a reversible, tight binding inhibitor of the human kinesin Eg5 that specifically blocks mitotic progression. *J. Biol. Chem.* **2006**, *281*, 17559–17569.

(15) Kozielski, F.; Skoufias, D. A.; Indorato, R. L.; Saoudi, Y.; Jungblut, P. R.; Hustoft, H. K.; Strozynski, M.; Thiede, B. Proteome analysis of apoptosis signaling by *S*-trityl-L-cysteine, a potent reversible inhibitor of human mitotic kinesin Eg5. *Proteomics* **2008**, *8*, 289–300.

(16) Ogo, N.; Oishi, S.; Matsuno, K.; Sawada, J.; Fujii, N.; Asai, A. Synthesis and biological evaluation of L-cysteine derivatives as mitotic kinesin Eg5 inhibitors. *Bioorg. Med. Chem. Lett.* **2007**, *17*, 3921–3924.

(17) Debonis, S.; Skoufias, D. A.; Indorato, R. L.; Liger, F.; Marquet, B.; Laggner, C.; Joseph, B.; Kozielski, F. Structure−activity relationship of *S*-trityl-L-cysteine analogues as inhibitors of the human mitotic kinesin Eg5. *J. Med. Chem.* **2008**, *51*, 1115–1125.

(18) Zee-Cheng, K. Y.; Cheng, C. C. Experimental antileukemic agents. Preparation and structure−activity study of *S*-tritylcysteine and related compounds. *J. Med. Chem.* **1970**, *13*, 414–418.

(19) Konig, W.; Geiger, R.; Siedel, W. New S-protecting groups for cystein. *Chem. Ber.* **1968**, *101*, 681–693.

(20) Marvel, C. S.; Dietz, F. C.; Himel, C. M. The dissociation of hexaarylethanes. XIII. Halogen substituents. *J. Org. Chem.* **1942**, *7*, 392–396.

(21) Murphy, D. J. Determination of accurate KI values for tight-binding enzyme inhibitors: an in silico study of experimental error and assay design. *Anal. Biochem.* **2004**, *327*, 61–67.

(22) Kaan, H. Y.; Ulaganathan, V.; Hackney, D. D.; Kozielski, F. An allosteric transition trapped in an intermediate state of a new kinesin−inhibitor complex. *Biochem. J.* **2010**, *425*, 55–60.

(23) Wiltshire, C.; Singh, B. L.; Stockley, J.; Fleming, J.; Doyle, B.; Barnetson, R.; Robson, C. N.; Kozielski, F.; Leung, H. Y. Docetaxel-resistant prostate cancer cells remain sensitive to *S*-trityl-L-cysteine-mediated Eg5 inhibition. *Mol. Cancer Ther.* **2010**, *9*, 1730–1739.

(24) Sakowicz, R.; Finer, J. T.; Beraud, C.; Crompton, A.; Lewis, E.; Fritsch, A.; Lee, Y.; Mak, J.; Moody, R.; Turincio, R.; Chabala, J. C.; Gonzales, P.; Roth, S.; Weitman, S.; Wood, K. W. Antitumor activity of a kinesin inhibitor. *Cancer Res.* **2004**, *64*, 3276–3280.

(25) Marcus, A. I.; Peters, U.; Thomas, S. L.; Garrett, S.; Zelnak, A.; Kapoor, T. M.; Giannakakou, P. Mitotic kinesin inhibitors induce mitotic arrest and cell death in Taxol-resistant and -sensitive cancer cells. *J. Biol. Chem.* **2005**, *280*, 11569–11577.

(26) Peters, T.; Lindenmaier, H.; Haefeli, W. E.; Weiss, J. Interaction of the mitotic kinesin Eg5 inhibitor monastrol with P-glycoprotein. *Naunyn Schmiedeberg's Arch. Pharmacol.* **2006**, *372*, 291–299.

(27) Cox, C. D.; Breslin, M. J.; Whitman, D. B.; Coleman, P. J.; Garbaccio, R. M.; Fraley, M. E.; Zrada, M. M.; Buser, C. A.; Walsh, E. S.; Hamilton, K.; Lobell, R. B.; Tao, W.; Abrams, M. T.; South, V. J.; Huber, H. E.; Kohl, N. E.; Hartman, G. D. Kinesin spindle protein (KSP) inhibitors. Part V: discovery of 2-propylamino-2,4-diaryl-2,5-dihydropyrroles as potent, water-soluble KSP inhibitors, and modulation of their basicity by beta-fluorination to overcome cellular efflux by P-glycoprotein. *Bioorg. Med. Chem. Lett.* **2007**, *17*, 2697–2702.

(28) Cox, C. D.; Coleman, P. J.; Breslin, M. J.; Whitman, D. B.; Garbaccio, R. M.; Fraley, M. E.; Buser, C. A.; Walsh, E. S.; Hamilton, K.; Schaber, M. D.; Lobell, R. B.; Tao, W.; Davide, J. P.; Diehl, R. E.; Abrams, M. T.; South, V. J.Huber, H. E.; Torrent, M.; Prueksaritanont, T.; Li, C.; Slaughter, D. E.; Mahan, E.; Fernandez-Metzler, C.; Yan, Y.; Kuo, L. C.; Kohl, N. E.; Hartman, G. D. Kinesin spindle protein (KSP) inhibitors. 9. Discovery of (2*S*)-4-(2,5-difluorophenyl)-*n*-[(3*R*,4*S*)-3-fluoro-1-methylpiperidin-4-yl]-2-(hydroxymethyl)-*N*-methyl-2-phenyl-2,5-dihydro-1*H*-pyrrole-1-carboxamide (MK-0731) for the treatment of taxane-refractory cancer. *J. Med. Chem.* **2008**, *51*, 4239–4352.

(29) *Gold Suite 1.0.1*; Cambridge Crystallographic Data Centre: Cambridge, UK, 2008.

(30) Kim, E. D.; Buckley, R.; Learman, S.; Richard, J.; Parke, C.; Worthylake, D. K.; Wojcik, E. J.; Walker, R. A.; Kim, S. Allosteric drug discrimination is coupled to mechanochemical changes in the kinesin-5 motor core. *J. Biol. Chem.* **2010**, *285*, 18650–18661.

(31) Zee-Cheng, K. Y.; Cheng, C. C. Structural modification of *S*-trityl-L-cysteine. Preparation of some *S*-(substituted trityl)-L-cysteines and dipeptides of *S*-trityl-L-cysteine. *J. Med. Chem.* **1972**, *15*, 13–16.

(32) Kessel, D.; Smith, G.; Blahnik, J. Effects of *S*-(trityl)-L-cysteine and its analogs on cell surface properties of leukemia L1210 cells. *Biochem. Pharmacol.* **1976**, *25*, 1893–1897.

(33) Paull, K. D.; Lin, C. M.; Malspeis, L.; Hamel, E. Identification of novel antimitotic agents acting at the tubulin level by computer-assisted evaluation of differential cytotoxicity data. *Cancer Res.* **1992**, *52*, 3892–3900.

(34) Brier, S.; Lemaire, D.; DeBonis, S.; Forest, E.; Kozielski, F. Molecular dissection of the inhibitor binding pocket of mitotic kinesin Eg5 reveals mutants that confer resistance to antimitotic agents. *J. Mol. Biol.* **2006**, *360*, 360–376.

(35) Brier, S.; Lemaire, D.; Debonis, S.; Forest, E.; Kozielski, F. Identification of the protein binding region of *S*-trityl-L-cysteine, a new potent inhibitor of the mitotic kinesin Eg5. *Biochemistry* **2004**, *43*, 13072–13082.

(36) Brier, S.; Lemaire, D.; DeBonis, S.; Kozielski, F.; Forest, E. Use of hydrogen/deuterium exchange mass spectrometry and mutagenesis as a tool to identify the binding region of inhibitors targeting the human mitotic kinesin Eg5. *Rapid Commun. Mass Spectrom.* **2006**, *20*, 456–462.

(37) Copeland, R. A. Tight binding inhibition. In *Evaluation of Enzyme Inhibitors in Drug Discovery*; John Wiley & Sons: New York, 2005; pp 178−213.

(38) Weiss, J.; Herzog, M.; Konig, S.; Storch, C. H.; Ketabi-Kiyanvash, N.; Haefeli, W. E. Induction of multiple drug transporters by efavirenz. *J. Pharmacol. Sci.* **2009**, *109*, 242–250.

(39) Weiss, J.; Dormann, S. M.; Martin-Facklam, M.; Kerpen, C. J.; Ketabi-Kiyanvash, N.; Haefeli, W. E. Inhibition of P-glycoprotein by newer antidepressants. *J. Pharmacol. Exp. Ther.* **2003**, *305*, 197–204.

(40) *Omega 2.2.1*, OpenEye Scientific Software: Santa Fe, NM, USA, 2007.

(41) *LigandScout 2.03*; Inte:Ligand GmbH: Vienna, 2009.

(42) Cruickshank, D. W. Remarks about protein structure precision. *Acta Crystallogr., Sect. D: Biol. Crystallogr.* **1999**, *55*, 583–601.